Nanoscale

REVIEW

View Article Online
View Journal | View Issue

Cite this: *Nanoscale*, 2021, **13**, 15142

Self-assembly of peptide nanofibers for imaging applications

Qiaochu Jiang,† Xiaoyang Liu, † Gaolin Liang * and Xianbao Sun*

Received 31st July 2021,
Accepted 1st September 2021

DOI: 10.1039/d1nr04992e

rsc.li/nanoscale

Pathological stimuli-responsive self-assembly of peptide nanofibers enables selective accumulation of imaging agent cargos in the stimuli-rich regions of interest. It provides enhanced imaging signals, biocompatibility, and tumor/disease accessibility and retention, thereby promoting smart, precise, and sensitive tumor/disease imaging both *in vitro* and *in vivo*. Considering the remarkable significance and recent encouraging breakthroughs of self-assembled peptide nanofibers in tumor/disease diagnosis, this reivew is herein proposed. We emphasize the recent advances particularly in the past three years, and provide an outlook in this field.

1. Introduction

Self-assembly of biocomponents is a crucial biological event for living objects. For example, proteins exhibit physiological functions in their assembled states (tertiary and quaternary structures).[1] Of note, abnormal assembly is always closely related to pathological changes, which may help indicate the occurrence of certain diseases (*e.g.*, self-assembly of amyloid-beta is responsible for Alzheimer's disease).[2] As a consequence, exploring the self-assembly behaviors of biocomponents can be conducive to understanding certain pathological events at the molecular level.[3,4] To this end, biomolecules, particularly peptides with self-assembly ability, are frequently employed as mimics for tumor/disease diagnosis.[5–7] Driven by thermodynamics and kinetics,[8] these peptides spontaneously form ordered assemblies (*e.g.*, nanoparticles, nanotubes, and nanofibers) through multiple noncovalent interactions between building blocks.[9,10]

Among these peptide assemblies, nanofibers have attracted intensive interest in tumor/disease imaging or therapy. First, in contrast to other assemblies (*e.g*, nanoparticles, nanomicelles, *etc*.), nanofibers possess much higher surface-area-to-volume ratios, which provide more functionable and active sites and allow better cooperative interactions with bio-targets, such as cellular mitochondria of tumor,[11] thus allowing enhanced tumor accessibility. Second, nanofibers show enhanced retention effects in tumor sites,[12] and may exhibit superior tumor accumulation than nanoparticles at the same size,[13] therefore facilitating sustained tumor/disease imaging or drug release. Third, intracellularly formed nanofibers may disturb the dynamics of microtubules of glioblastoma cells,[14] while pericellular nanofibers can decrease the migration of several cancer cells (*e.g.*, HeLa),[15] thus nanofibers hold promise as platforms for fabricating novel theranostic agent. Last and most importantly, nanofibers could further gel water to form supramolecular hydrogels, which are considered as highly promising versatile biomaterials with prominent loading capacity, biocompatibility, and biodegradability for broad applications such as drug delivery, cell culture, and bioimaging.[16]

To date, self-assembled peptide nanofibers have been recognized as attractive and promising carriers of various imaging agents for smart and precise tumor/disease imaging.[17–22] Conjugated with imaging agents,[23–25] peptide precursors were rationally designed with responsiveness to tumor/disease-related over-expressed pathological stimuli, such as alkaline phosphatase (ALP),[26] matrix metalloproteinase-2 (MMP-2),[27] and bacteria surface receptors.[28] As such, *in situ* self-assembly of nanofibers could be smartly activated. This process enabled the smart localization and accumulation of the imaging agents at the target site of interest, thus promoting precise and sensitive imaging.[29,30] Moreover, in contrast to the inactivated small-molecule peptide precursors in less-/non-stimuli healthy cells, nanofibers formed in tumor/disease cells could prolong the intracellular retention time of the imaging agents, thus affording enhanced metabolism difference, specificity and sustainability of imaging. Considering that smart self-assembled peptide nanofibers have shown remarkable significance in tumor/disease diagnosis, and notable breakthroughs in this field particularly in the past three years have not been emphatically reviewed, we herein provide this review. We highlighted the recent advance in smart self-assembly of rationally designed nanofibers,

State Key Laboratory of Bioelectronics, School of Biological Science and Medical Engineering, Southeast University, 2 Sipailou Road, Nanjing 210096, China. E-mail: gliang@seu.edu.cn, xbsun@seu.edu.cn
† These authors contributed equally to this work.

which enabled enhanced imaging of tumor/disease with modalities including magnetic resonance imaging (MRI), optical imaging (OI), photoacoustic imaging (PAI), and multi-modality imaging. We anticipate this review will inspire more designs of smart peptide nanofibers for enhanced tumor/disease diagnosis.

2. Self-assembly of nanofibers for imaging applications

2.1 Design principles of smart peptide nanofiber precursors for imaging applications

Smart peptide nanofiber precursors consist of two parts: (1) self-assembly unit, and (2) stimulus–cleavable blocking unit (Scheme 1). Once activated by the stimulus, the self-assembly unit would act as the building block to form nanofibers.

Self-assembly unit. Some common features can be found in prevalent self-assembly units of peptide nanofibers, such as supramolecular interactions (*e.g.*, hydrogen bonding, π–π stacking, and hydrophobic interactions) and β-sheet secondary structure. However, it remains challenging to precisely predict whether a designated peptide sequence could self-assemble into nanofibers. As a result, molecular design of peptide self-assembly units mainly relies on modifying known motifs. Currently, most well-known nanofiber-forming peptide units are derived from or inspired by natural proteins (*e.g.*, β-amyloid). For example, long β-sheet-forming amphiphilic peptides with alternating hydrophilic/hydrophobic (or positively/negatively charged) amino acids, such as naturally occurring EAK16 peptide (AEAEAKAKAEAEAKAK)[31] and its variant RADA16 (RADARADARADARADA).[32] To form nanofibers with these peptides, factors including peptide concentration, temperature, pH, and ionic profile need to be seriously considered.[33] In the past two decades, enormous efforts have been made to explore short peptide (less than ten residues) building blocks of nanofibers,[34] aiming to reduce the complexity in peptide design and synthesis, and facilitate the study of underlying sequence-structure–property relationships. Since being discovered by Reches and Gazit from the core self-assembling peptide sequence of β-amyloid,[35] the di-phenylalanine (FF) has been recognized as the minimal β-sheet-forming peptide motif that can self-assemble into nanofibers. This self-assembly process is driven by forces of the hydrogen bonding between the peptide backbones and the π–π stacking between the aromatic phenyl groups. By varying the sequence type or length, various FF derivative peptides (*e.g.*, IF, FFF, KFFE) have also been experimentally testified as feasible building blocks for self-assembly of nanofibers.[36] In recent years, hydrophobic and aromatic moieties, such as 9-fluorenylmethyloxycarbonyl (Fmoc),[37] and naphthyl (Nap),[38] are frequently coupled with FF or its derivatives in order to introduce additional driving forces (*i.e.*, hydrophobic and π–π stacking interactions) in a synergistic manner, thus promoting rapid self-assembly kinetics and robust physicochemical properties of nanofibers. Owing to their high programmability and simplicity in structure, synthesis, and scaling up, short aromatic FF derivatives have been most frequently employed as peptide building blocks for designing smart nanofiber precursors (Table 1).

Stimulus–cleavable blocking unit. This unit makes materials "smart" by activating the loaded imaging or therapeutic agents exclusively with the predesignated stimuli, thus enabling precise imaging or therapy of tumor/disease.[39–43] Stimulus–cleavable chemistry has provided considerable stimulus-substrate pairs for on-demand design of smart materials.[44] In regard to the fabrication of stimulus-responsive nanofiber precursors, substrate moieties conjugated to the self-assembly units should be capable of blocking the self-assembly of nanofibers, as well as specifically responding to the stimuli (Table 1). For example, to design smart FF-based nanofiber precursors, substrates with comparable hydrophilicity (*e.g.*, $Y(H_2PO_3)$[45]) are commonly chosen to make precursors amphiphilic. As such, these precursors would be in molecular state or form nanoparticles, which would form or transform into nanofibers *in situ* once triggered by the corresponding stimuli (*e.g.*, alkaline phosphatase).

2.2 Self-assembly of nanofibers for MRI

Magnetic resonance imaging (MRI) is one of the most prevalent clinical non-invasive diagnostic tools with deep penetration and high spatial resolution.[46] In magnetic field, teeny changes in body can significantly influence the relaxation parameters of hydrogen or fluorine nuclei, and further generate MRI signals.[47] Nevertheless, MRI still need contrast agents (CAs) as adjuvants to improve its sensitivity in handling clinical issues. According to the ratio between longitudinal relaxation (r_1) and transverse relaxation (r_2), CAs are mainly divided into T_1 and T_2 agents. T_1 agents produce positive contrast, and are commonly based on stable and inert paramagnetic ions, such as gadolinium (Gd).[48] T_2 agents produce negative contrasts, and are based on complexes such as superparamagnetic iron oxide (SPIO).[25]

Small molecular Gd-based CAs were proved that they can increase the ^1H relaxation rates of nearby water molecules, thereby enhancing MRI contrast signals.[24] However, these CAs were subject to fast body clearance after administration, thus showing limited retention ability. To address this issue, Gd-based nanomaterials have been proposed, such as polymers, nanoparticles, micelles, liposomes and nanofibers.[47,49–51] For example, Zhang *et al.* designed a MMP-2-responsive peptide Ppdf-Gd that enabled nanosphere-to-nanofiber transformation in tumor microenvironment (Fig. 1a).[52] In brief, the amphiphi-

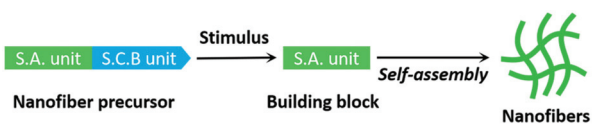

Scheme 1 Smart peptide nanofiber precursors for imaging applications. S.A. unit, self-assembly unit; S.C.B unit, stimulus–cleavable blocking unit.

Table 1 Representative stimulus-responsive peptide nanofiber precursors for bioimaging

Nanofiber precursor	Peptide self-assembly unit		Stimulus–cleavable blocking unit	Stimulus	Imaging application	Ref.
	Sequence	Driving force				
NBD-FF-easter-taurine	FF	Hydrogen bonding, π–π stacking	Ester bond	Esterase	Fluorescence imaging of Cellular esterase	56
Fmoc-K(FITC)FFY(H_2PO_3)	Fmoc-KFF	Hydrogen bonding, π–π stacking, hydrophobic interactions	Y(H_2PO_3)	Alkaline phosphatase (ALP)	Fluorescence imaging of tumor	57
Nap-FFK(DYKDDDDK)-NBD	Nap-FF	Hydrogen bonding, π–π stacking, hydrophobic interactions	DYKDDDDK	Enterokinase (ENTK)	Fluorescence imaging of ENTK activity	58
Nap-GFFK(Cou)Y(H_2PO_3)D	Nap-GFF	Hydrogen bonding, π–π stacking, hydrophobic interactions	Y(H_2PO_3)	Alkaline phosphatase (ALP)	Luminescence imaging of tumor	59
NBD-FFFGK(succ)G	FFF	Hydrogen bonding, π–π stacking	Succinylated K	SIRT5	Fluorescence imaging of mitochondria	60
Nap-FFFYp-EDA-DOTA(Gd)	Nap-FFF	Hydrogen bonding, π–π stacking, hydrophobic interactions	Y(H_2PO_3)	Alkaline phosphatase (ALP)	Magnetic resonance imaging of tumor	61
PpiX-PEG_8-SSSPLGLAK(DOTA)-PEG_6-F_4	FFFF	Hydrogen bonding, π–π stacking	PLGLA	Matrix metalloproteinase-2 (MMP-2)	Magnetic resonance imaging of tumor	52
GTDTKTGPAKLVFFC(Cyanine) TDTG	KLVFF	Hydrogen bonding, π–π stacking	GPA	FAP-α	Fluorescence imaging of tumor	62
RGDRDDRDDPLGYLGFFC(Cy)	YLGFFC	Hydrogen bonding, π–π stacking	PLGYLG	Matrix metalloproteinase-2/9 (MMP-2/9)	Fluorescence imaging of renal cell carcinoma	63
AVPIAQKDEVDKLVFFAEC(Cy)G	KLVFFAECG	Hydrogen bonding, π–π stacking	DEVD	Caspase-3/7	Fluorescence imaging of tumor	64
$mPEG_{2000}$-KLDLKLDLKLDL-p-SCN-deferoxamine-^{89}Zr	KLDLKLDLKLDL	Hydrophobic&electrostatic interactions	N-terminal K	Cathepsin B	Fluorescence/positron emission tomography/computed tomography imaging of tumor	65
Mannose-YVHDCKK(A-purpurin18)	K(A-purpurin18)	π–π stacking, hydrophobic interactions	YVHDC	Caspase-1	Photoacoustic imaging of tumor	66
Purpurin18-PLGVRGRGD	Purpurin18-PLG	π–π stacking, hydrophobic interactions	PLGVRG	Gelatinase	Photoacoustic imaging of tumor	12

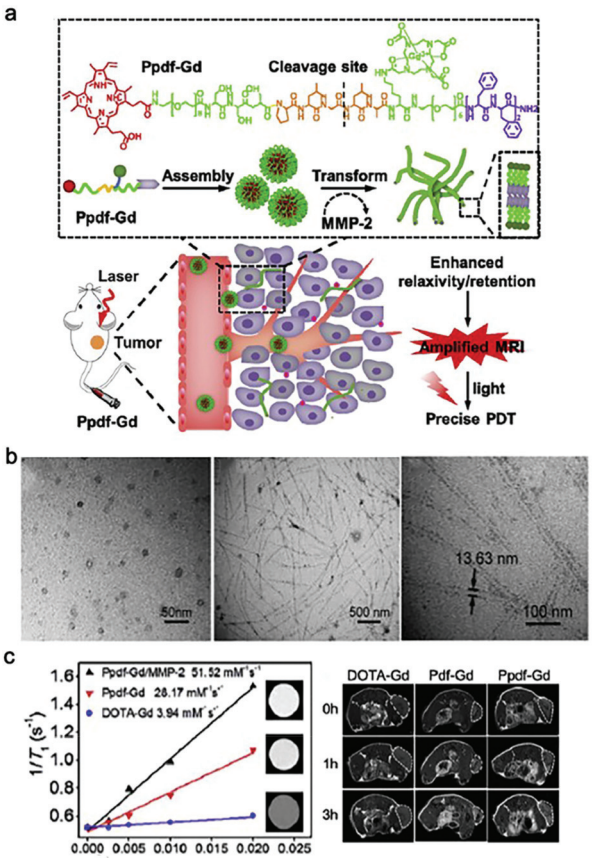

Fig. 1 (a) Schematic illustration of MMP-2-triggered transformation of Ppdf-Gd from spherical nanoparticles to nanofibers and the principle of dual-stage-amplified MRI and PDT. Ppdf-Gd can self-assembly to spherical nanoparticles in physiological conditions. When reaching tumor tissue by the EPR effect, the nanoparticles underwent sphere-to-fibers transformation under MMP-2. This transformation can enhance relaxivity and retention of contrast agent in tumor region, which realized amplified MRI and precise PDT. (b) TEM images of Ppdf-Gd solution in the presence or the absence of MMP-2 and amplified TEM image of Ppdf-Gd. (c) Left: longitudinal relaxation rates measurement of Ppdf-Gd, DOTA-Gd, and Ppdf-Gd with enzyme MMP-2. The insets represented the T1 weighted MR images of various groups at same Gd^{3+}concentration; Right: *T*1-weighted MRI images of mice at 0, 1, and 3 h after intravenous (i.v.) injection (Gd^{3+}dose: 0.05 mmoL kg^{-1}). Modified with permission from ref. 52. Copyright 2018. Elsevier Ltd.

lic Ppdf-Gd first self-assembled into spherical nanoparticles in physiological conditions to ensure efficient tumor accumulation due to EPR effect. Then the overexpressed MMP-2 in tumor microenvironment recognized and cleaved the peptide backbone, breaking the amphiphilicity and enabling the transformation from nanosphere to nanofiber (Fig. 1b), which further improved the retention time of the CAs. More importantly, this nanosphere-to-nanofiber transformation led to increased relaxation rate of the loaded DOTA-Gd, which afforded amplified tumor MRI signals than the control groups (*i.e.*, free DOTA-Gd, and MMP-2-inert Pdf-Gd) (Fig. 1c). Notably, this strategy utilized *in situ* morphology transformation (nanoparticle-to-nanofiber) to enhance the retention ability and MR signal of CA, which has shown merits as an attractive methodology for smart delivery of drugs or imaging agents.[53] However, for the Phe-Phe-based short peptides, their self-assembly tendency would be significantly impaired after modification with Gd complex.[54] To demonstrate this issue, Diaferia *et al.* replaced the Phe with more aromatic naphthylalanine, and proposed a dinaphthylalanine-Gd-conjugate (DOTA-L_6-2Nal_2) to form MRI nanofibers.[55]

Recently, chemical exchange saturation transfer (CEST)-based MRI has emerged as a highly promising strategy for tumor/disease imaging, owing to its enhanced sensitivity, natural labeling of bioactive molecules, and negligible background interference.[67,68] Cui *et al.* conjugated a peptide precursor with pemetrexed, an FDA-approved anticancer drug, as well as a CEST agent.[69] This conjugate could self-assemble into nanofibers in tumors, enabling enhanced tumor CEST MRI. Of note, traditional ^{1}H MRI are commonly limited by inherent noise interference from water molecules.[70] By contrast, ^{19}F MRI has shown great advantages due to its high sensitivity, wide chemical shift and negligible background.[71] For example, Liang group designed a smart ^{19}F nanofiber that was formed through ALP-instructed self-assembly, enabling sensitive MRI of enzyme activity *in vitro* and in cell lysates.[72]

2.3 Self-assembly of nanofibers for OI

Optical imaging (OI) is a non-invasive imaging modality that utilizes light including ultraviolet, visible and infrared regions.[73] OI can provide images of tissues and cells with high spatial resolution, but the resolution decreases rapidly with the increment of imaging depth.[74] Bioluminescence imaging (BI) and fluorescence imaging (FI) are the two most commonly used techniques. Considering that self-assembled peptide nanofibers for BI have seldom been reported, we thereby only summarize their FI applications.

Recently, He *et al.* designed a branched peptide (D-1$\bar{T}$FLAG) for targeting and enhanced imaging of mitochondria (Fig. 2a).[58] This peptide precursor firstly formed nanoparticles, which could target mitochondria due to their negative charges. Upon the cleavage by enterokinase (ETNK) expressed on the membrane of mitochondria, nanoparticles transfromed into nanofibers by self-assembly on mitochondria membrane (Fig. 2b). As such, the NBD dye, which exhibited aggregation-enhanced emission, efficiently accumulated on mitochondria, and produced enhanced fluorescence signals in tumor cells (Fig. 2c and d). Notably, mitochondria-targeting nanofiber precursor provided significant benefits to the enhancement of fluorescence signals. This is because precursors could be further concentrated after being internalized by mitochondria from cytoplasm, promoting the self-assembly of nanofibers. As a result, subcellular nanofiber precursors that target organelles may be advantageous and deserve to be developed for enhanced bioimaging. Of note, in contrast to conventional fluorescent dyes that are subjected to aggregation-caused quenching effect, NBD shows advantages in helping visualizing *in vivo* biological events with self-assembled peptide nanofibers. For example, Zhang *et al.* con-

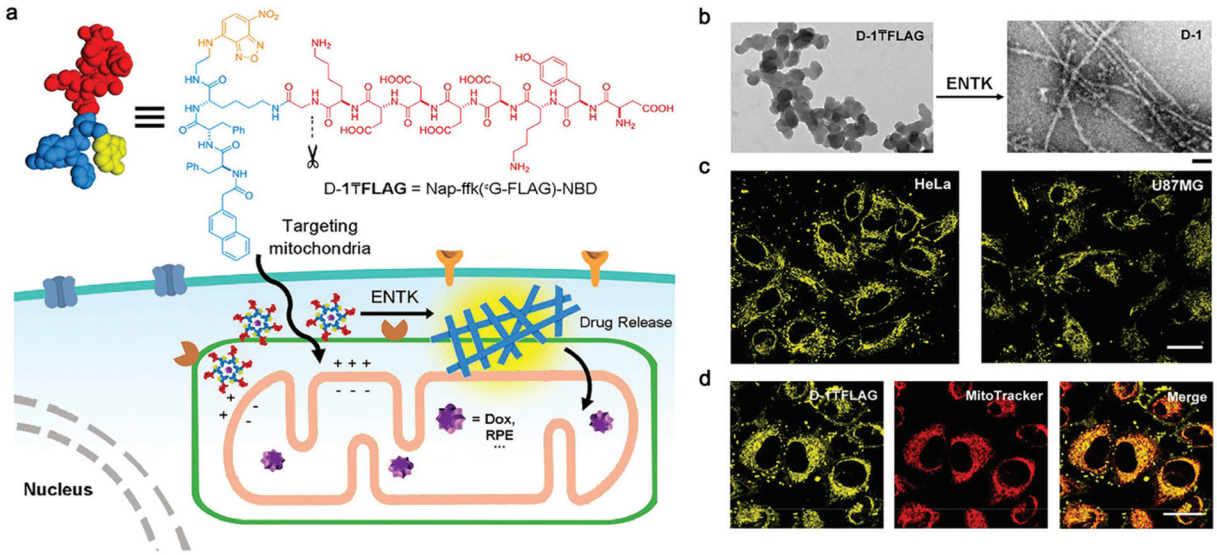

Fig. 2 (a) Structure of a representative branched peptide and ENTK cleaving the branch to convert micelles to nanofibers on mitochondria. (b) TEM images of D-1T̄FLAG before (left) and after (right) adding ENTK (24 h), scale bar = 100 nm. (c) Fluorescent images of HeLa and U87MG cells incubated with D-1T̄FLAG for 2 h. (d) The fluorescent images of D-1TFLAG and mitotracker in HeLa cells. Scale bar = 30 μm in panels c and d. The concentrations of D-1T̄FLAG are 200 μM for b–d. Modified with permission from ref. 58. Copyright 2018. American Chemical Society.

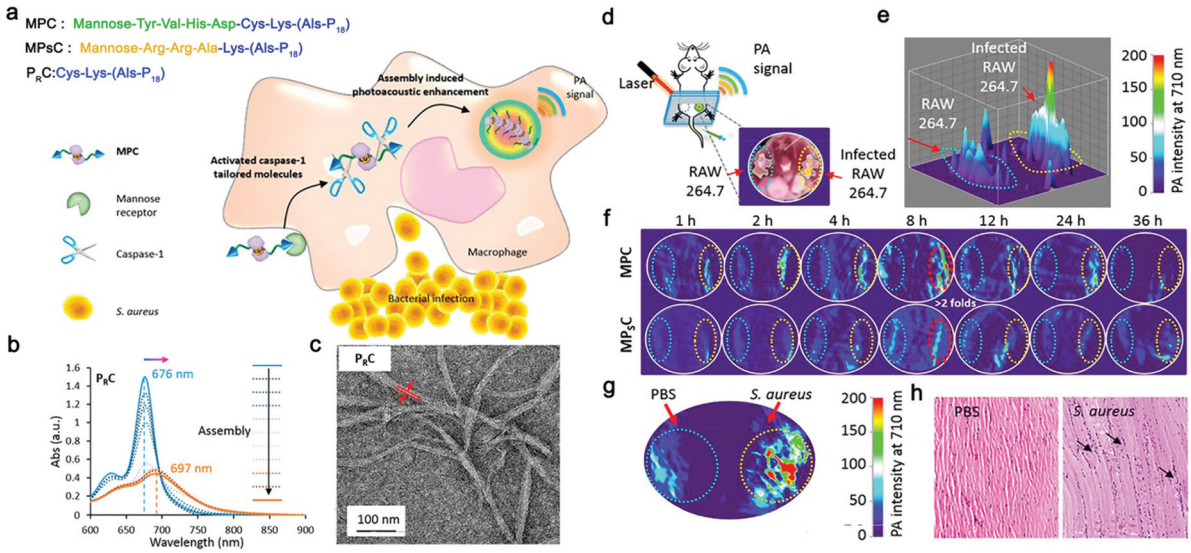

Fig. 3 (a) Schematic representation of macrophage chemotaxis-instructed *S. aureus* infection detection *in vivo* and the molecular component of the probe (MPC). Structure illustration of MPC, MP_SC and P_RC. (b) The UV–vis spectra of assembly procedure of molecule PRC in the mixture solution (H_2O/DMSO) with different volume ratios (from 0% to 100%). The molecule concentration is 5×10^{-5} M. (c) Transmission electron microscope (TEM) image of PRC fibrous assemblies in the aqueous solution (H_2O/DMSO; 95/5; v/v). (d) Chemotaxis-instructed *S. aureus* infection PA detection *in vivo*. Schematic illustration of the mice model (intramuscular injection of infected RAW 264.7 cells) and photoacoustic tomography (PAT) detection. The infected RAW 264.7 cells were obtained with the same procedure as before. The mice model was built after intramuscular injection of infected RAW 264.7 (10^7 cells per injection) for 12 h. (e) PA signal intensity distribution of infected RAW 264.7 cells *in vivo* after MPC administration with a dose of 35 mg kg^{-1} though i.v. injection for 8 h. (f) PA images of intracellular infection *in vivo* between 1 and 36 h after i.v. administration of MPC and MP_SC (35 mg kg^{-1}), respectively. The PA intensities per area of MPC and MPSC were calculated based on the red dotted circle area. (g) PA images of muscular infection. The right leg was infected after intramuscular injection of 108 cfu *S. aureus* cells for 12 h. (h) Representative micrographs of the histology of the muscle sections (H&E staining) of the *S. aureus* infected and the control (PBS) groups. Black arrows indicate the leukocytes during inflammation of the *S. aureus* invasion. The number of mice in each group is three. Modified with permission from ref. 66. Copyright 2018. American Chemical Society.

jugated NBD on a ALP- and GSH-responsive peptide nanofiber precursor, and achieved fluorescence "on/off" monitoring with the tandem assembly/disassembly of nanofibers in living tumor cells.[75] Alternatively, aggregation-induced emission (AIE) dyes also can be employed for the same imaging purpose.[76,77]

However, autofluorescence interference and inferior tissue penetration of visible light still largely limit the applications of fluorescent nanofibers in visualizing deep-situated biological events.[78] Considering that absorption and scattering ability of biological tissues to photons attenuated rapidly with the increment of light wavelength, NIR light may significantly improve tissue penetration and spatial resolution of imaging.[79] In recent years, numerous NIR imaging probes or nanomaterials have been developed. For example, Zhao *et al.* constructed a smart NIR peptide probe for improved tumor imaging.[62] This probe was consisted of two hydrophilic motifs, a tailoring motif, a self-assembly motif, and a NIR cyanine dye. Upon the specific cleavage by fibroblast activation protein-α (FAP-α), the probe would be activated and self-assemble into nanofibers on the surface of tumor-associated fibroblasts (CAFs). Self-assembled nanofibers were confirmed *in vitro*. Notably, *in vivo* results demonstrated that self-assembly of nanofibers provided significantly enhanced retention effect and sustained imaging capacity.

2.4 Self-assembly of nanofibers for PAI

Photoacoustic imaging (PAI) is a non-invasive imaging method that combines optical excitation with ultrasonic detection based on photoacoustic effect.[80] Compared with traditional OI, PAI owns higher spatial resolution and improved tissue penetration depth (several centimeters deep in biological tissue imaging).[81] However, only a few natural light absorbers exists, such as melanin and hemoglobin, while others are not able to send out photoacoustic signals.[82] Therefore, various exogenous photoacoustic agents, particularly smart photoacoustic nanomaterials, have been developed to enhance the photoacoustic contrast. For example, Pu's group reported a self-assembled semiconducting polymer amphiphile (SPA).[83] As a near-infrared absorbing material, this SPA showed advantages in stability, fluorescence quantum yield, and tumor-targeting ability, enabling precise and sensitive tumor PAI. Remarkably, Liang's group proposed an ALP-responsive NIR probe, which could self-assembled in ALP-rich tumor cells, achieving smart and enhanced *in vivo* PAI of tumor.[84]

Recently, Wang's group proposed a smart chlorophyll-peptide-based photoacoustic agent (MPC) for imaging intracellular bacterial infection, which was responsible for relevant treatment failure and potential antibiotic resistance.[66] This MPC was consisted of a macrophage-targeting motif, a caspase-1-cleavable tailoring motif and a chlorophyll-Cu^{2+}

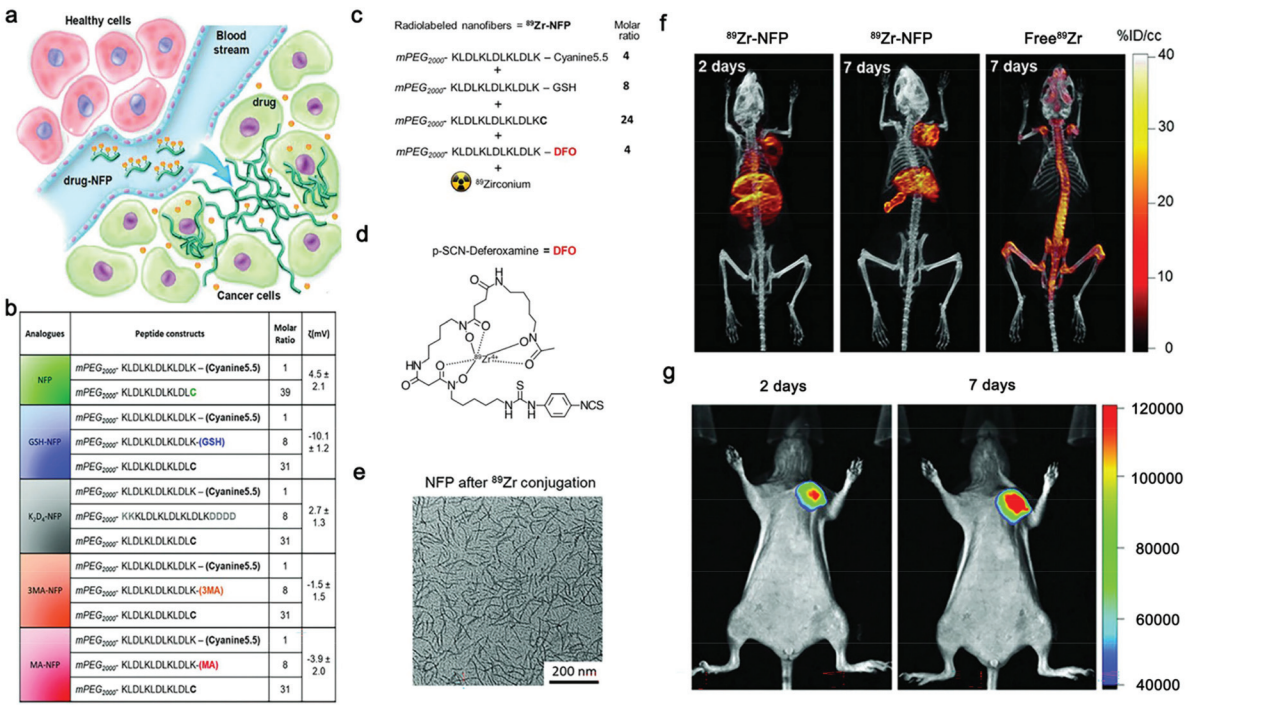

Fig. 4 (a) Design of advanced NFP analogues to enhance tumoral uptake, penetration, and local retention. NFP has a high aspect ratio that promotes its uptake by solid tumors. Multiple NFPs can penetrate tumor tissue and subsequently transform into larger interfibril networks *via in situ* activation by tumor-associated proteases, thus minimizing lymphatic clearance. When used for drug delivery, NFP prolongs the drug–tumor contact time to achieve more effective treatment. (b) A table showing the peptide composition and surface charge (zeta potential) of the NFP analogues. The peptide derivatives were used to coassemble the nanofibers. (c) Synthesis of a dual Cyanine5.5- and ^{89}Zr-labeled GSH-NFP (^{89}Zr-NFP) for studying the biodistribution by fluorescence/PET/CT imaging. The ratio of different peptide constructs used for assembling ^{89}Zr-NFP. Deferoxamine (DFO) served as the chelator of ^{89}Zr. (d) Molecular structure of DFO. (e) TEM analysis of GSH-NFP after DFO-^{89}Zr conjugation. Representative PET/CT whole body images of SCID mice bearing MDA-MB-468 tumors were acquired 2 and 7 days after injection of 100 μCi of ^{89}Zr-NFP or free ^{89}Zr-oxylate as the control (n = 3 per group). Representative fluorescence whole body images of SCID mice bearing MDA-MB-468 tumors (n = 4) 2 and 7 days after IV injection of ^{89}Zr-NFP (100 μCi). Modified with permission from ref. 65. Copyright 2018, Wiley-VCH GmbH.

coordination PA signal motif (Fig. 3a). When infected by bacteria, macrophage immediately expressed caspase-1, which cleaved MPC and activated its self-assembly, further forming nanofibers and quenching the fluorescence (Fig. 3b and c). In the mouse model that was constructed by injecting infected macrophage cells (Fig. 3d), approximately 2.6-fold higher PAI signals were observed upon infection than that of the healthy group (Fig. 3e), and reached the maximum intensity at 8 h (Fig. 3f). The *S. aureus* infection model verified the chemotaxis-instructed infection of PA detection (Fig. 3g). The infected muscles stained by H&E (Fig. 3h) indicated the inflammation of the *S. aureus* invasion. This work provided inspirations for PAI of bacterial infection and even the related diseases with smart self-assembled peptide nanofibers. Considering that various peptide nanofibers have been used as advantageous carriers of antimicrobial therapeutic agents,[85] it would be promising to combine PAI imaging and therapy agents on smart nanofiber precursors for novel antimicrobial theranostics.

2.5 Self-assembly of nanofibers for multi-modality imaging

In recent years, intensive interest has been raised to develop multi-modality techniques to combine the advantages of various imaging modalities. Smart nanomaterials have been frequently employed as carriers to load multimodal imaging agents. For example, gold nanoparticles were conjugated with the peptide substrate of MMP-2 for smart PET/CT imaging of tumor;[86] ALP-responsive Fe_3O_4-based nanoparticles were proposed for smart MR/Optical Imaging;[87] DOTA-Gd and a NIR fluorophore were conjugated on ALP-responsive self-assembling dipeptide for smart and sensitive NIR/MR imaging.[88]

Peptide nanofibers has been explored for multimodal imaging of tumor. For example, Law *et al.* reported a peptide precursor (NFP) which was capable of self-assembling into nanofibers in tumor regions (Fig. 4a).[65] As a carrier, the NFP provided design flexibility for on-demand customization of imaging/therapy agents (Fig. 4b). The optimized GSH-NFP could realize real-time monitoring tumoral delivery by loading Cy5.5 or DFO (Fig. 4c and d). After the cleavage of hydrophilic mPEG by tumor-associated proteases (*e.g.*, cathepsin B), ^{89}Zr-NFP conjugate could self-assemble into large nanofibers (Fig. 4e), providing improved cancer targeting and tissue invasion ability, and enhanced FI/PET/CT multi-modality imaging of tumor (Fig. 4f and g). However, in this work modality agents were not conjugated on one nanofiber precursor, thus a set of precursor analogues were necessitated to realize multi-modality imaging of tumor, which rendered complicated synthesis and less accurate administration of the imaging agents. Unfortunately, smart nanofiber precursors with integrated modality agents still remain to be developed for precise imaging of tumor/disease with the highly promising multi-modality technique.

3. Conclusion and outlook

In this review, we summarized the recent progress on smart self-assembled nanofibers for tumor/disease imaging with various modalities, including magnetic resonance imaging (MRI), optical imaging (OI), photoacoustic imaging (PAI), and multi-modality imaging. These nanofibers were smartly formed through *in situ* self-assembly of the peptide building blocks, which were activated by tumor/disease-related pathological stimuli of interest (*e.g.*, enzyme). As such, imaging agents loaded on nanofibers were able to accumulate in the stimuli-rich regions with improved tumor/disease accessibility, retention, and metabolism difference, thereby enabling smart, precise, and sensitive tumor/disease imaging both *in vitro* and *in vivo*.

Nevertheless, some challenges remain to be addressed in this field. First, given that the level and activity of stimuli may differ across types and species ascribed to tumor/disease heterogeneity, therefore highly specific and robust pathological stimuli of tumor/disease of interest still need to be explored for programming more smart nanofibers with reliable responsiveness. Second, nanofibers may transform their morphologies in complicated *in vivo* conditions due to their dynamic and reversible nature,[9,10] thus impairing their properties. As a result, systematical insights into their behaviors in physiological context should be taken to correlate them with their building blocks, which would help establish new design principles of smart nanofiber precursors. More importantly, long-term *in vivo* pharmacokinetics and biosafety of nanofibers should be strictly evaluated and addressed to promote their clinical translation. Inspiringly, self-assembled peptide nanofibers also show great potential in theranostics[89] and therapeutics[64,90] of tumor/disease. With this review, we anticipate efforts from multidisciplinary researchers could be devoted to advance the development and clinical translation of smart self-assembled nanofibers for precise and enhanced tumor/disease diagnosis and therapy.

Conflicts of interest

There are no conflicts to declare.

Acknowledgements

This work was supported by the National Natural Science Foundation of China (Grants 21725505 and 22074016), and the China Postdoctoral Science Foundation funded project (2020M671303).

References

1 J. Wang, K. Liu, R. Xing and X. Yan, *Chem. Soc. Rev.*, 2016, **45**, 5589–5604.
2 Y. J. Chung, K. Kim, B. I. Lee and C. B. Park, *Small*, 2017, **13**, 1700983.
3 M. Kaplan, P. Subramanian, D. Ghosal, C. M. Oikonomou, S. Pirbadian, R. Starwalt-Lee, S. K. Mageswaran,

D. R. Ortega, J. A. Gralnick, M. Y. El-Naggar and G. J. Jensen, *EMBO J.*, 2019, **38**, e100957.
4 R. Kubota, S. Liu, H. Shigemitsu, K. Nakamura, W. Tanaka, M. Ikeda and I. Hamachi, *Bioconjugate Chem.*, 2018, **29**, 2058–2067.
5 J. Li and K. Pu, *Chem. Soc. Rev.*, 2019, **48**, 38–71.
6 Y. Deng, W. Zhan and G. Liang, *Adv. Healthcare Mater.*, 2021, **10**, e2001211.
7 Q. Miao and K. Pu, *Adv. Mater.*, 2018, **30**, e1801778.
8 W. Zhang, X. Yu, Y. Li, Z. Su, K. D. Jandt and G. Wei, *Prog. Polym. Sci.*, 2018, **80**, 94–124.
9 J. Song, R. Xing, T. Jiao, Q. Peng, C. Yuan, H. Mohwald and X. Yan, *ACS Appl. Mater. Interfaces*, 2018, **10**, 2368–2376.
10 V. Castelletto, J. Seitsonen, K. M. Tewari, A. Hasan, R. M. Edkins, J. Ruokolainen, L. M. Pandey, I. W. Hamley and K. H. A. Lau, *ACS Macro Lett.*, 2020, **9**, 494–499.
11 D. B. Cheng, X. H. Zhang, Y. J. Gao, L. Ji, D. Hou, Z. Wang, W. Xu, Z. Y. Qiao and H. Wang, *J. Am. Chem. Soc.*, 2019, **141**, 7235–7239.
12 D. Zhang, G. B. Qi, Y. X. Zhao, S. L. Qiao, C. Yang and H. Wang, *Adv. Mater.*, 2015, **27**, 6125–6130.
13 A. Wagh, J. Singh, S. Qian and B. Law, *Nanomedicine*, 2013, **9**, 449–457.
14 Y. Kuang and B. Xu, *Angew. Chem., Int. Ed.*, 2013, **52**, 6944–6948.
15 Y. Kuang, J. Shi, J. Li, D. Yuan, K. A. Alberti, Q. Xu and B. Xu, *Angew. Chem., Int. Ed.*, 2014, **53**, 8104–8107.
16 X. Liu, X. Sun and G. Liang, *Biomater. Sci.*, 2021, **9**, 315–327.
17 F. Zhang, Y. Ma, Y. Chi, H. Yu, Y. Li, T. Jiang, X. Wei and J. Shi, *Sci. Rep.*, 2018, **8**, 8208.
18 B. J. Kim and B. Xu, *Bioconjugate Chem.*, 2020, **31**, 492–500.
19 P. Wang, Y. Fan, L. Lu, L. Liu, L. Fan, M. Zhao, Y. Xie, C. Xu and F. Zhang, *Nat. Commun.*, 2018, **9**, 2898.
20 Y. Li, G. Liu, J. Ma, J. Lin, H. Lin, G. Su, D. Chen, S. Ye, X. Chen, X. Zhu and Z. Hou, *J. Controlled Release*, 2017, **258**, 95–107.
21 C. F. Anderson and H. Cui, *Ind. Eng. Chem. Res.*, 2017, **56**, 5761–5777.
22 X. Hu, F. Li, S. Wang, F. Xia and D. Ling, *Adv. Healthcare Mater.*, 2018, **7**, e1800359.
23 Z. Zhou, Z. Han and Z. R. Lu, *Biomaterials*, 2016, **85**, 168–179.
24 Z. Cai, C. Wu, L. Yang, D. Wang and H. Ai, *ACS Biomater. Sci. Eng.*, 2020, **6**, 2533–2542.
25 C. Diaferia, E. Gianolio and A. Accardo, *J. Pept. Sci.*, 2019, **25**, e3157.
26 Z. Hai and G. Liang, *Adv. Biosyst.*, 2018, **2**, 1800108.
27 N. J. W. Penfold, J. Yeow, C. Boyer and S. P. Armes, *ACS Macro Lett.*, 2019, **8**, 1029–1054.
28 S. Long, Q. Qiao, L. Miao and Z. Xu, *Chin. Chem. Lett.*, 2019, **30**, 573–576.
29 L. Wang, C. Gong, X. Yuan and G. Wei, *Nanomaterials*, 2019, **9**, 285.
30 L. J. Chen and H. B. Yang, *Acc. Chem. Res.*, 2018, **51**, 2699–2710.
31 S. Zhang, T. Holmes, C. Lockshin and A. Rich, *Proc. Natl. Acad. Sci. U. S. A.*, 1993, **90**, 3334–3338.
32 T. C. Holmes, S. d. Lacelle, X. Su, G. S. Liu, A. Rich and S. G. Zhang, *Proc. Natl. Acad. Sci. U. S. A.*, 2000, **97**, 6728–6733.
33 F. Gelain, Z. Luo and S. Zhang, *Chem. Rev.*, 2020, **120**, 13434–13460.
34 Y. Zhao, W. Yang, C. Chen, J. Wang, L. Zhang and H. Xu, *Curr. Opin. Colloid Interface Sci.*, 2018, **35**, 112–123.
35 M. Reches and E. Gazit, *Science*, 2003, **300**, 625–627.
36 A. Lampel, R. V. Ulijn and T. Tuttle, *Chem. Soc. Rev.*, 2018, **47**, 3737–3758.
37 K. Tao, A. Levin, L. Adler-Abramovich and E. Gazit, *Chem. Soc. Rev.*, 2016, **45**, 3935–3953.
38 Y. Zhang, Y. Kuang, Y. Gao and B. Xu, *Langmuir*, 2011, **27**, 529–537.
39 J. Huang, J. Li, Y. Lyu, Q. Miao and K. Pu, *Nat. Mater.*, 2019, **18**, 1133–1143.
40 Y. Zhang, S. He, W. Chen, Y. Liu, X. Zhang, Q. Miao and K. Pu, *Angew. Chem., Int. Ed.*, 2021, **60**, 5921–5927.
41 S. He, J. Li, Y. Lyu, J. Huang and K. Pu, *J. Am. Chem. Soc.*, 2020, **142**, 7075–7082.
42 P. Cheng, W. Chen, S. Li, S. He, Q. Miao and K. Pu, *Adv. Mater.*, 2020, **32**, e1908530.
43 C. Zhang, Z. Zeng, D. Cui, S. He, Y. Jiang, J. Li, J. Huang and K. Pu, *Nat. Commun.*, 2021, **12**, 2934.
44 Y. Xue, H. Bai, B. Peng, B. Fang, J. Baell, L. Li, W. Huang and N. H. Voelcker, *Chem. Soc. Rev.*, 2021, **50**, 4872–4931.
45 J. Gao, J. Zhan and Z. Yang, *Adv. Mater.*, 2020, **32**, e1805798.
46 P. Padmanabhan, A. Kumar, S. Kumar, R. K. Chaudhary and B. Gulyas, *Acta Biomater.*, 2016, **41**, 1–16.
47 A. Babic, V. Vorobiev, G. Trefalt, L. A. Crowe, L. Helm, J. P. Vallee and E. Allemann, *Chem. Commun.*, 2019, **55**, 945–948.
48 J. Elistratova, B. Akhmadeev, V. Korenev, M. Sokolov, I. Nizameev, A. Gubaidullin, A. Voloshina and A. Mustafina, *Soft Matter*, 2018, **14**, 7916–7925.
49 P. Xie, P. Du, J. Li and P. Liu, *Carbohydr. Polym.*, 2019, **205**, 377–384.
50 Y. Yuan, J. Zhang, X. Qi, S. Li, G. Liu, S. Siddhanta, I. Barman, X. Song, M. T. McMahon and J. W. M. Bulte, *Nat. Mater.*, 2019, **18**, 1376–1383.
51 R. An, X. Cheng, S. Wei, Y. Hu, Y. Sun, Z. Huang, H. Y. Chen and D. Ye, *Angew. Chem., Int. Ed.*, 2020, **59**, 20636–20644.
52 J. Zhang, Y. L. Mu, Z. Y. Ma, K. Han and H. Y. Han, *Biomaterials*, 2018, **182**, 269–278.
53 L. Zhang, D. Jing, N. Jiang, T. Rojalin, C. M. Baehr, D. Zhang, W. Xiao, Y. Wu, Z. Cong, J. J. Li, Y. Li, L. Wang and K. S. Lam, *Nat. Nanotechnol.*, 2020, **15**, 145–153.
54 C. Diaferia, E. Gianolio, P. Palladino, F. Arena, C. Boffa, G. Morelli and A. Accardo, *Adv. Funct. Mater.*, 2015, **25**, 7003–7016.

55 C. Diaferia, E. Gianolio, T. Sibillano, F. A. Mercurio, M. Leone, C. Giannini, N. Balasco, L. Vitagliano, G. Morelli and A. Accardo, *Sci. Rep.*, 2017, **7**, 307.
56 J. Zhou, X. Du, J. Li, N. Yamagata and B. Xu, *J. Am. Chem. Soc.*, 2015, **137**, 10040–10043.
57 L. Dong, Q. Miao, Z. Hai, Y. Yuan and G. Liang, *Anal. Chem.*, 2015, **87**, 6475–6478.
58 H. He, J. Wang, H. Wang, N. Zhou, D. Yang, D. R. Green and B. Xu, *J. Am. Chem. Soc.*, 2018, **140**, 1215–1218.
59 Y. Zhong, J. Zhan, G. Xu, Y. Chen, Q. Qin, X. Liao, S. Ma, Z. Yang and Y. Cai, *Angew. Chem., Int. Ed.*, 2021, **60**, 8121–8129.
60 L. Yang, R. Peltier, M. Zhang, D. Song, H. Huang, G. Chen, Y. Chen, F. Zhou, Q. Hao, L. Bian, M. L. He, Z. Wang, Y. Hu and H. Sun, *J. Am. Chem. Soc.*, 2020, **142**, 18150–18159.
61 L. Dong, J. Qian, Z. Hai, J. Xu, W. Du, K. Zhong and G. Liang, *Anal. Chem.*, 2017, **89**, 6922–6925.
62 X. X. Zhao, L. L. Li, Y. Zhao, H. W. An, Q. Cai, J. Y. Lang, X. X. Han, B. Peng, Y. Fei, H. Liu, H. Qin, G. Nie and H. Wang, *Angew. Chem., Int. Ed.*, 2019, **58**, 15287–15294.
63 H. W. An, D. Hou, R. Zheng, M. D. Wang, X. Z. Zeng, W. Y. Xiao, T. D. Yan, J. Q. Wang, C. H. Zhao, L. M. Cheng, J. M. Zhang, L. Wang, Z. Q. Wang, H. Wang and W. Xu, *ACS Nano*, 2020, **14**, 927–936.
64 R. Zheng, J. Yang, M. Mamuti, D. Y. Hou, H. W. An, Y. Zhao and H. Wang, *Angew. Chem., Int. Ed.*, 2021, **60**, 7809–7819.
65 V. Bellat, R. Ting, T. L. Southard, L. Vahdat, H. Molina, J. Fernandez, O. Aras, T. Stokol and B. Law, *Adv. Funct. Mater.*, 2018, **28**, 1803969.
66 Q. Cai, Y. Fei, L. Hu, Z. Huang, L. L. Li and H. Wang, *Nano Lett.*, 2018, **18**, 6229–6236.
67 K. M. Ward, A. H. Aletras and R. S. Balaban, *J. Magn. Reson.*, 2000, **143**, 79–87.
68 G. Liu, X. Song, K. W. Chan and M. T. McMahon, *NMR Biomed.*, 2013, **26**, 810–828.
69 L. L. Lock, Y. Li, X. Mao, H. Chen, V. Staedtke, R. Bai, W. Ma, R. Lin, Y. Li, G. Liu and H. Cui, *ACS Nano*, 2017, **11**, 797–805.
70 I. Tirotta, V. Dichiarante, C. Pigliacelli, G. Cavallo, G. Terraneo, F. B. Bombelli, P. Metrangolo and G. Resnati, *Chem. Rev.*, 2015, **115**, 1106–1129.
71 X. Tang, X. Gong, A. Li, H. Lin, C. Peng, X. Zhang, X. Chen and J. Gao, *Nano Lett.*, 2020, **20**, 363–371.
72 Z. Zheng, H. Sun, C. Hu, G. Li, X. Liu, P. Chen, Y. Cui, J. Liu, J. Wang and G. Liang, *Anal. Chem.*, 2016, **88**, 3363–3368.
73 J. Song, X. Yang, Z. Yang, L. Lin, Y. Liu, Z. Zhou, Z. Shen, G. Yu, Y. Dai, O. Jacobson, J. Munasinghe, B. Yung, G. J. Teng and X. Chen, *ACS Nano*, 2017, **11**, 6102–6113.
74 G. D. Luker and K. E. Luker, *J. Nucl. Med.*, 2008, **49**, 1–4.
75 M. Zhang, C. Wang, C. Yang, H. Wu, H. Xu and G. Liang, *Anal. Chem.*, 2021, **93**, 5665–5669.
76 Y. Qian, W. Wang, Z. Wang, X. Jia, Q. Han, I. Rostami, Y. Wang and Z. Hu, *ACS Appl. Mater. Interfaces*, 2018, **10**, 7871–7881.
77 A. Han, H. Wang, R. T. Kwok, S. Ji, J. Li, D. Kong, B. Z. Tang, B. Liu, Z. Yang and D. Ding, *Anal. Chem.*, 2016, **88**, 3872–3878.
78 Kenry, Y. Duan and B. Liu, *Adv. Mater.*, 2018, **30**, e1802394.
79 Y. Hu, Y. Wang, X. Wen, Y. Pan, X. Cheng, R. An, G. Gao, H. Y. Chen and D. Ye, *Research*, 2020, **2020**, 4087069.
80 P. Beard, *Interface Focus*, 2011, **1**, 602–631.
81 S. R. Kothapalli, T. J. Ma, S. Vaithilingam, O. Oralkan, B. T. Khuri-Yakub and S. S. Gambhir, *IEEE Trans. Biomed. Eng.*, 2012, **59**, 1199–1204.
82 A. Dragulescu-Andrasi, S. R. Kothapalli, G. A. Tikhomirov, J. Rao and S. S. Gambhir, *J. Am. Chem. Soc.*, 2013, **135**, 11015–11022.
83 C. Xie, X. Zhen, Q. Lei, R. Ni and K. Pu, *Adv. Funct. Mater.*, 2017, **27**, 1605397.
84 C. Wu, R. Zhang, W. Du, L. Cheng and G. Liang, *Nano Lett.*, 2018, **18**, 7749–7754.
85 B. Hu, C. Owh, P. L. Chee, W. R. Leow, X. Liu, Y. L. Wu, P. Guo, X. J. Loh and X. Chen, *Chem. Soc. Rev.*, 2018, **47**, 6917–6929.
86 W. Mao, H. S. Kim, Y. J. Son, S. R. Kim and H. S. Yoo, *J. Controlled Release*, 2018, **269**, 52–62.
87 X. R. Song, S. H. Li, J. Dai, L. Song, G. Huang, R. Lin, J. Li, G. Liu and H. H. Yang, *Small*, 2017, **13**, 1603997.
88 R. Yan, Y. Hu, F. Liu, S. Wei, D. Fang, A. J. Shuhendler, H. Liu, H. Y. Chen and D. Ye, *J. Am. Chem. Soc.*, 2019, **141**, 10331–10341.
89 N. Liu, L. Zhu, Z. Li, W. Liu, M. Sun and Z. Zhou, *Biomater. Sci.*, 2021, **9**, 5427–5436.
90 E. Arslan, I. C. Garip, G. Gulseren, A. B. Tekinay and M. O. Guler, *Adv. Healthcare Mater.*, 2014, **3**, 1357–1376.